Composite Structures 372 (2025) 119615

Contents lists available at ScienceDirect

Composite Structures

journal homepage: www.elsevier.com/locate/compstruct

DSQK finite element with assumed orthogonality bending energy and mixed transverse shear strains for thermal buckling analysis of three-layer functionally graded sandwich plates

Irwan Katili [a,*], Sundararajan Natarajan [b], Magd Abdel Wahab [c,d,e], Susilo Widyatmoko [a]

[a] Universitas Indonesia, Depok 16424, Indonesia
[b] Pandurangan Faculty Fellow, Department of Mechanical Engineering, Indian Institute of Technology Madras, Chennai 600036 Tamil Nadu, India
[c] Laboratory Soete, Faculty of Engineering and Architecture, Ghent University, Technologiepark Zwijnaarde 46 B-9052 Zwijnaarde, Belgium
[d] College of Engineering, Yuan Ze University, Taiwan
[e] Parallel and Distributed Systems Laboratory, Jožef Stefan Institute, Jamova cesta 39, SI-1000 Ljubljana, Slovenia

ARTICLE INFO

Keywords:
DSQK quadrilateral element
Assumed orthogonality bending energy
Mixed transverse shear strains
Thermal buckling
FSDT
FGM

ABSTRACT

Thermal buckling of three-layer functionally graded sandwich plates is numerically studied using a new modified discrete shear quadrilateral plate element called the DSQK element. The plate kinematics is based on the Mindlin-Reissner formulation, and the proposed plate element has five degrees of freedom per node. To pass the constant bending strain patch test, an assumed orthogonality in bending strain energy is adopted from Bergan's free formulation. The shear locking is alleviated by mixed transverse shear strains that are expressed by the second derivative of rotations obtained from the kinematic relationship, constitutive law, and equilibrium equations. The proposed element is valid for both thin and thick plates. The accuracy and the robustness of the proposed element are demonstrated with a few numerical examples. Furthermore, the influence of the plate aspect ratio, material gradient index, various schemes and thicknesses of three-layer functionally graded sandwich plates on the thermal buckling behaviour is studied.

1. Introduction

Functionally graded materials (FGMs) are engineered materials known for their custom-tailorable properties to meet the requirements. The FGMs are typically made up of two constituents, viz., metal and ceramic. The metallic constituent provides ductility, and the ceramic constituent provides a thermal barrier and anti-corrosive property, which protects the FGM from metal corrosion [1]. Due to their custom-tailorable mechanical properties, the FGMs have found their application in various fields of engineering and science as they are characterised by the smooth and continuous variation in the properties from one surface to another. As the FGMs provide structural integrity, from both the mechanical and thermal perspectives, they are preferred over isotropic plates and fibre-reinforced laminated composites, especially in critical areas where compressive loads can cause instability. Therefore, it is crucial to select an effective plate theory to accurately predict buckling under various loading conditions, as well as geometric and material properties. Amongst various engineered structures, sandwich-type structures are preferred, especially in aerospace applications. Sandwich structures typically have a core and two facesheets; this offers better fatigue resistance, low specific weight, improved vibration characteristics and bending rigidity compared to a uniform-thickness material. The presence of a core and two facesheets introduces interfaces where the material properties change abruptly. However, when FGMs are employed, the facesheet-core interface is eliminated, as a gradual variation in the material properties is achievable.

One of the distinctive advantages of FGMs is that they act as thermal barriers. To understand the thermal response, several researchers have examined the response of FGM sandwich plates to thermal buckling using different plate theories and numerical approaches.

For robust and accurate prediction of the realistic behaviour of sandwich structures, a full three-dimensional analysis is computationally demanding, which has attracted researchers to explore two-dimensional plate theories for predicting the structural response. Amongst the available theories, classical plate theory (CPT) or Kirchhoff plate theory [2] and first-order shear deformation theory (FSDT) or

* Corresponding author.
E-mail address: irwan.katili@ui.ac.id (I. Katili).

https://doi.org/10.1016/j.compstruct.2025.119615
Received 2 May 2025; Received in revised form 15 August 2025; Accepted 20 August 2025
Available online 23 August 2025

Reissner-Mindlin [3,4] plate theory are predominantly used. In CPT plate theory, plate buckling is governed by a single equation containing the general out-of-plane displacement field w and the in-plane load (N_x, N_y). In the FSDT model, buckling behaviour is governed by three independent equations (w, β_x, β_y) and the applied plane load (N_x, N_y). FSDT has the advantage of theoretical simplicity and is capable of providing accurate results for moderately thick plates. However, it is limited in its ability to accurately model thicker plates because the transverse shear stress distribution is assumed to vary constantly along the thickness direction and therefore requires a shear correction factor to correctly represent the strain energy deformation. For numerical study, FSDT is preferred over CPT and has been found to be applicable in almost all commercial finite element software, such as Abaqus, Ansys, etc. This could be attributed to the fact that CPT requires C^1 continuous functions, whilst FSDT relaxes this constraint and requires only C^0 continuous functions, which makes it amenable to the finite element code. However, this flexibility poses additional challenges; for example, to represent the transverse shear energy accurately, a shear correction factor $\kappa = 5/6$ is required [5–19]. The available literature for the mechanical response of FGM plates using the FSDT can be found in [20–31]. Moreover, when the finite element formulation based on FSDT is applied to thin plates, the numerical results show spurious oscillations, commonly referred to as shear-locking pathology.

To avoid shear correction factors, the high-order shear deformation theory (HSDT) was introduced by Reddy in the 1980s [32–34] to account for the parabolic distribution of transverse shear strains, which can handle thicker, layered composite plates well. HSDT provides a more accurate representation of the distribution of shear stress and strain across the thickness, thereby improving accuracy in bending and buckling analysis. An HSDT called Carrera's Unified Formulation (CUF) [35] was developed for multilayer plates in which the displacement vector, stress, and strain tensors are expanded in terms of the coordinates of the thickness. The development of HSDT on FGM plates can be studied in [36–48]. The Generalized Unified Formulation (GUF) is a method for creating a wide range of structural theories for plates and shells, particularly for composite materials. It provides a systematic way to generate a wide range of theories, including Equivalent Single Layer (ESL), Zig-Zag, and Layer-Wise (LW) theories [46]. A more sophisticated composite structure model called the Sublaminate Generalized Unified Formulation (S-GUF), particularly useful for sandwich panels, allows building any desired thickness expansion with any function [48]. Despite the more accurate results due to accounting for the parabolic distribution of the transverse shear stresses, HSDT requires more computational resources.

This study proposes an extension of Katili's recently introduced DSQK element [5], as an improvement of the DSQ element, to analyse the critical thermal buckling of FGM sandwich plates. Research on thermal buckling in FGM plates can be found in [49–56]. The proposed element offers accuracy, shear locking-free, and proper rank. The plate kinematics is modelled using the simple FSDT with a constant shear correction factor $\kappa = 5/6$, the discrete shear method using mixed transverse shear strain [6], and an assumed orthogonality condition for bending energy [7,8]. The domain is discretised with 4-noded bilinear elements, each with 5 degrees of freedom per node. For thermal buckling analysis, the von Kármán kinematic model is employed, and three models of temperature rise are used, i.e., uniform temperature rise (UTR), linear temperature rise (LTR), and nonlinear temperature rise (NLTR). The influence of the material gradient index based on the power law model, plate aspect, and thickness ratio is systematically studied. The results of the numerical study are presented by comparing those obtained from the current framework with other numerical results [55,56].

In Section 2, the formulation of the DSQK plate element for the FGM sandwich and thermal buckling analysis is introduced. The reliability of the proposed DSQK element with various schemes of FGM sandwich plate problems and its comparison with the solutions available in the literature based on analytical and/or other numerical methods are presented in Section 3.

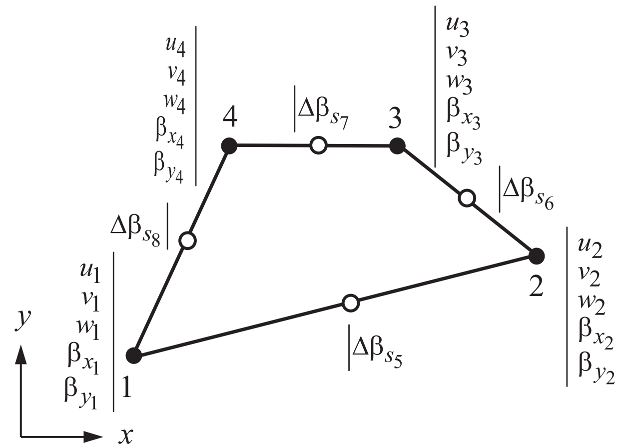

Fig. 1. A DSQK plate element with five final DOFs at each corner node and one temporary DOF at each mid-side node.

2. Formulation of DSQK element for FGM plates

In the FGM plates, the membrane-bending action occurs due to unsymmetrical material through the thickness. Hence, the DSQK element for the FGM plates has 5 DOFs (u_i, v_i, w_i, β_{x_i}, β_{y_i}) at corner nodes i ($i = 1, 2, 3, 4$), and one temporary DOF at each mid-side node k ($k = 5, 6, 7, 8$) of the element ($\Delta\beta_{s_k}$) (Fig. 1). These temporary degrees of freedom are needed to increase the rotation functions from linear to quadratic and will be eliminated later.

2.1. Basic equations of Reissner-Mindlin plates

The membrane strains:

$$\{e\} = \begin{Bmatrix} e_x \\ e_y \\ e_{xy} \end{Bmatrix} = \begin{Bmatrix} \dfrac{\partial u}{\partial x} \\ \dfrac{\partial v}{\partial y} \\ \dfrac{\partial u}{\partial y} + \dfrac{\partial v}{\partial x} \end{Bmatrix} \tag{1}$$

The bending strains:

$$\{\chi\} = \begin{Bmatrix} \chi_x \\ \chi_y \\ \chi_{xy} \end{Bmatrix} = \begin{Bmatrix} \dfrac{\partial \beta_x}{\partial x} \\ \dfrac{\partial \beta_y}{\partial y} \\ \dfrac{\partial \beta_x}{\partial y} + \dfrac{\partial \beta_y}{\partial x} \end{Bmatrix} \tag{2}$$

The kinematic transverse shear strains:

$$\{\gamma\} = \begin{Bmatrix} \gamma_{xz} \\ \gamma_{yz} \end{Bmatrix} = \begin{Bmatrix} \gamma_x \\ \gamma_y \end{Bmatrix} = \begin{Bmatrix} \beta_x + \dfrac{\partial w}{\partial x} \\ \beta_y + \dfrac{\partial w}{\partial y} \end{Bmatrix} \tag{3}$$

The equilibrium equations for the internal forces acting on the mid-surface:

$$\begin{aligned} T_x &= M_{x,x} + M_{xy,y} \\ T_y &= M_{y,y} + M_{xy,x} \end{aligned} \tag{4}$$

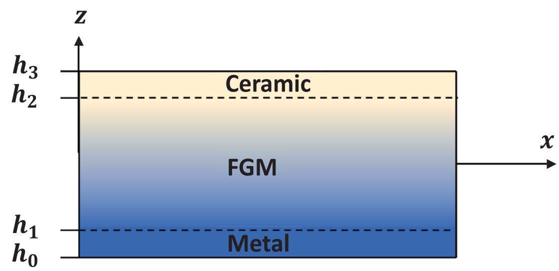

Fig. 2. FGM sandwich scheme 1-6-1.

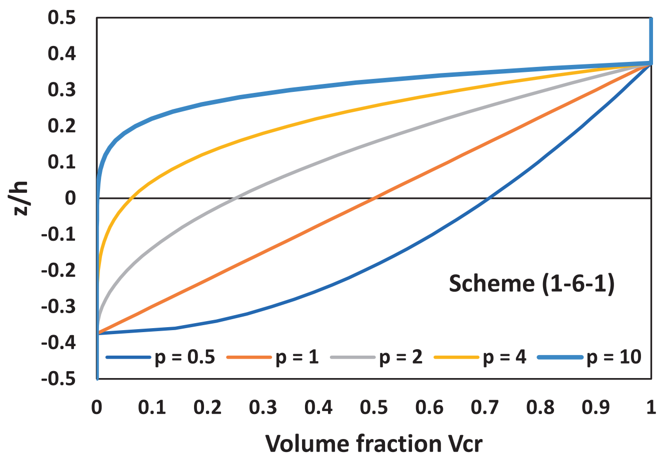

Fig. 3. The volume fraction of FGM sandwich plates.

2.2. Material properties of FGM plates

The material properties of FGM plates are generally not symmetrical to the middle surface ($z = 0$); thus, a couple of membranes and bending strain energies appear.

In the z-direction, the material properties vary continuously following a power law function such that:

$$\begin{aligned} E^n(z) &= E_{cr}V^n_{cr}(z) + E_{mt}V^n_{mt}(z) \\ \alpha^n(z) &= \alpha_{cr}V^n_{cr}(z) + \alpha_{mt}V^n_{mt}(z) \\ K^n(z) &= K_{cr}V^n_{cr}(z) + K_{mt}V^n_{mt}(z) \\ & V^n_{cr}(z) + V^n_{mt}(z) = 1 \end{aligned} \tag{5}$$

where $E^n(z)$, $\alpha^n(z)$, and $K^n(z)$ are the functions of the Young modulus, thermal expansion coefficient, and thermal conductivity coefficient at the n-layer. E_{cr} and E_{mt} are the elastic properties of ceramic and metal. α_{cr} and α_{mt} are the thermal expansion coefficients of ceramic and metal. K_{cr} and K_{mt} are the thermal conductivity coefficients of ceramic and metal, respectively. $V^n_{cr}(z)$ and $V^n_{mt}(z)$ are the volume fractions of ceramic and metal at n-layer, respectively.

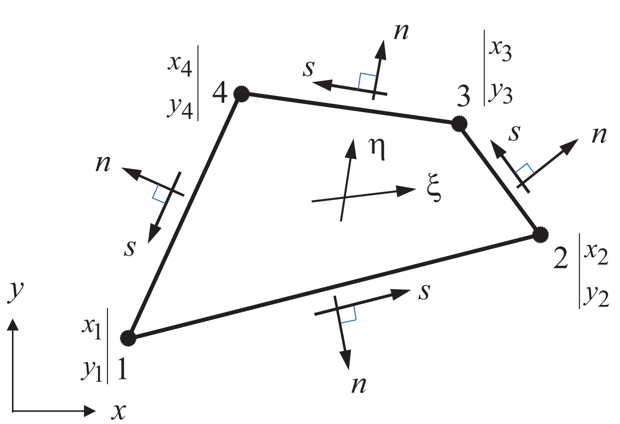

Fig. 4. Geometric of DSQK element in Cartesian (x-y), parametric (ξ-η), and normal-tangential (n-s) systems.

In this paper, the FGM sandwich plates (Fig. 2) are pure metal at the lower layer (h_0–h_1) and pure ceramic at the upper (h_2–h_3) layer. The core is an FGM with properties that vary from h_1 (metal) to h_2 (ceramic).

The volume fraction of the FGM sandwich plates is defined:

$$\text{Metal } (h_0 \leqslant z \leqslant h_1):\ V^1_{cr}(z) = 0\ ;\ V^1_{mt}(z) = 1$$

$$\text{FGM } (h_1 \leqslant z \leqslant h_2): \begin{cases} V^2_{cr}(z) = \left(\dfrac{z - h_1}{h_2 - h_1}\right)^p \\ V^2_{mt}(z) = 1 - \left(\dfrac{z - h_1}{h_2 - h_1}\right)^p \end{cases} \tag{6}$$

$$\text{Ceramic } (h_2 \leqslant z \leqslant h_3):\ V^3_{cr}(z) = 1\ ;\ V^3_{mt}(z) = 0$$

The ceramic volume fraction for FGM sandwich plates with scheme 1-6-1 is illustrated in Fig. 3.

2.3. Internal forces

The internal forces in FGM sandwich plates are defined through the following equations:

Membrane forces:

$$\{N\} = \begin{Bmatrix} N_x \\ N_y \\ N_{xy} \end{Bmatrix} = [H_m]\begin{Bmatrix} e_x \\ e_y \\ e_{xy} \end{Bmatrix} + [H_{mb}]\begin{Bmatrix} \chi_x \\ \chi_y \\ \chi_{xy} \end{Bmatrix} \tag{7}$$

Bending moments:

$$\{M\} = \begin{Bmatrix} M_x \\ M_y \\ M_{xy} \end{Bmatrix} = [H_{mb}]\begin{Bmatrix} e_x \\ e_y \\ e_{xy} \end{Bmatrix} + [H_b]\begin{Bmatrix} \chi_x \\ \chi_y \\ \chi_{xy} \end{Bmatrix} \tag{8}$$

Shear forces:

$$\{T\} = \begin{Bmatrix} T_x \\ T_y \end{Bmatrix} = [H_s]\begin{Bmatrix} \gamma_x \\ \gamma_y \end{Bmatrix} \tag{9}$$

where

$$\begin{aligned} [H_m] &= D_m\begin{bmatrix} 1 & \upsilon & 0 \\ \upsilon & 1 & 0 \\ 0 & 0 & (1-\upsilon)/2 \end{bmatrix} \\ [H_{mb}] &= D_{mb}\begin{bmatrix} 1 & \upsilon & 0 \\ \upsilon & 1 & 0 \\ 0 & 0 & (1-\upsilon)/2 \end{bmatrix} \\ [H_b] &= D_b\begin{bmatrix} 1 & \upsilon & 0 \\ \upsilon & 1 & 0 \\ 0 & 0 & (1-\upsilon)/2 \end{bmatrix} \\ [H_s] &= D_s\begin{bmatrix} 1 & 0 \\ 0 & 1 \end{bmatrix} \end{aligned} \tag{10}$$

$[H_m]$, $[H_{mb}]$, $[H_b]$, $[H_s]$ are the constitutive matrices for membrane, couple membrane-bending, bending, and transverse shear, respectively. D_m, D_{mb}, D_b, D_s are the membrane, couple membrane-bending, bending, and shear rigidity coefficients, respectively, and for FGM sandwich plates, are calculated as follows:

$$D_m = \frac{1}{(1-\upsilon^2)}\sum_{n=1}^{3}\int_{h_{n-1}}^{h_n} E^n(z)dz$$
$$D_{mb} = \frac{1}{(1-\upsilon^2)}\sum_{n=1}^{3}\int_{h_{n-1}}^{h_n} zE^n(z)dz$$
$$D_b = \frac{1}{(1-\upsilon^2)}\sum_{n=1}^{3}\int_{h_{n-1}}^{h_n} z^2E^n(z)dz \tag{11}$$
$$D_s = \frac{\kappa}{2(1+\upsilon)}\sum_{n=1}^{3}\int_{h_{n-1}}^{h_n} E^n(z)dz$$

where υ and κ are the Poisson's ratio and the transverse shear correction factor, respectively, which, for the sake of simplicity in this paper, are assumed constant in the z-direction.

E^n is the modulus of elasticity (5) at layer n, h_n is the plate thickness layer n.

2.4. Jacobian matrix and its inverse

The arbitrary points in the quadrilateral element are defined as follows (Fig. 4),

$$x = \sum_{i=1}^{4} N_i x_i \; ; \; y = \sum_{i=1}^{4} N_i y_i \tag{12}$$

$$N_i = \frac{1}{4}(1+\xi_i\xi)(1+\eta_i\eta) \tag{13}$$

$-1 \le \xi \le 1$ and $-1 \le \eta \le 1$ are the parametric coordinate systems. ξ_i and η_i are the nodal coordinates i in the parametric systems.

The Jacobian matrix $[J]$ and its inverse $[j]$ can be obtained from (12) to (13) as follows:

$$[J] = \begin{bmatrix} J_{11} & J_{12} \\ J_{21} & J_{22} \end{bmatrix} = \begin{bmatrix} \frac{\partial x}{\partial \xi} & \frac{\partial y}{\partial \xi} \\ \frac{\partial x}{\partial \eta} & \frac{\partial y}{\partial \eta} \end{bmatrix}$$
$$[j] = \begin{bmatrix} j_{11} & j_{12} \\ j_{21} & j_{22} \end{bmatrix} = \frac{1}{\det[J]}\begin{bmatrix} J_{22} & -J_{12} \\ -J_{21} & J_{11} \end{bmatrix} \tag{14}$$

2.5. Membrane strains and stiffness

The displacements u in the x-direction and v in the y-direction are defined as follows:

$$u = \sum_{i=1}^{4} N_i u_i \; ; \; v = \sum_{i=1}^{4} N_i v_i \tag{15}$$

The linear shape functions N_i are given in (13).

Substituting (15) into the membrane strains (1), we get:

$$\{e\} = [B_m]\{u_n\}$$
$$[B_m] = \begin{bmatrix} & \frac{\partial N_i}{\partial x} & 0 & 0 & 0 & 0 & \\ \cdots & 0 & \frac{\partial N_i}{\partial y} & 0 & 0 & 0 & \ldots i = 1,2,3,4 \\ & \frac{\partial N_i}{\partial y} & \frac{\partial N_i}{\partial x} & 0 & 0 & 0 & \end{bmatrix} \tag{16}$$

$$\langle u_n \rangle = \langle \cdots \; u_i \; v_i \; w_i \; \beta_{x_i} \; \beta_{y_i} \; \cdots \rangle_{i=1,4} \tag{17}$$

The energy and stiffness for the membrane are given by:

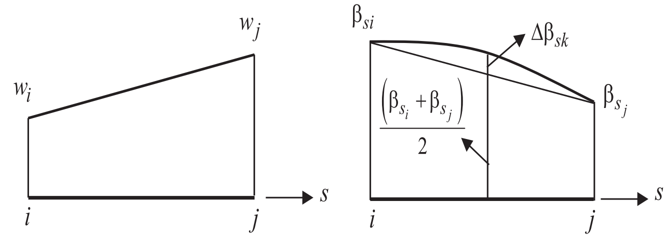

Fig. 5. Deflection w and rotations in s direction.

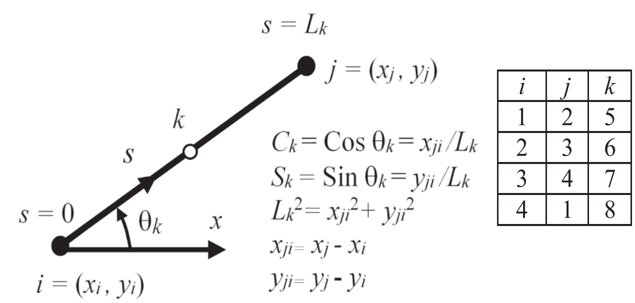

Fig. 6. C_k and S_k on side k in tangential s coordinate system.

$$\Pi_{int}^{m} = \frac{1}{2}\int_A \langle e \rangle [H_m]\{e\} dA = \frac{1}{2}\langle u_n \rangle [k_m]\{u_n\}$$
$$[k_m] = \int_A [B_m]^T [H_m]\ [B_m] dA \tag{18}$$

$[H_m]$ is the constitutive matrix for membrane forces in FGM plates (10).

2.6. Bending strains, energy, and stiffness

The deflection w and rotation β_s alongside s (i-j) are expressed as:

$$w(s) = \left(1 - \frac{s}{L_k}\right) w_i + \frac{s}{L_k} w_j$$
$$\beta_s = \left(1 - \frac{s}{L_k}\right)\beta_{s_i} + \left(\frac{s}{L_k}\right)\beta_{s_j} + 4\frac{s}{L_k}\left(1 - \frac{s}{L_k}\right)\Delta\beta_{s_k} \tag{19}$$

where w and β_s are the linear and quadratic functions in s. (Fig. 5).

Based on (19), the displacements w, rotations β_x, and rotation β_y are:

$$w = \sum_{i=1}^{4} N_i w_i$$
$$\beta_x = \sum_{i=1}^{4} N_i \beta_{x_i} + \sum_{k=5}^{8} P_k C_k \Delta\beta_{s_k} \tag{20}$$
$$\beta_y = \sum_{i=1}^{4} N_i \beta_{y_i} + \sum_{k=5}^{8} P_k S_k \Delta\beta_{s_k}$$

C_k and S_k are given in Fig. 6. The linear functions N_i are given in (13), and the quadratic functions P_k are given in (21).

$$P_5 = \frac{1}{2}(1-\xi^2)(1-\eta) \; ; \; P_6 = \frac{1}{2}(1+\xi)(1-\eta^2)$$
$$P_7 = \frac{1}{2}(1-\xi^2)(1+\eta) \; ; \; P_8 = \frac{1}{2}(1-\xi)(1-\eta^2) \tag{21}$$

By substituting (20) into (2), the bending strains will then be separated into two matrices $[B_{b_u}]$ and $[B_{b_\Delta}]$

$$\{\chi\} = [B_{b_u}]\{u_n\} + [B_{b_\Delta}]\{\Delta\beta_{s_n}\}$$
$$\langle \Delta\beta_{s_n} \rangle = \langle \Delta\beta_{s_5} \;\; \Delta\beta_{s_6} \;\; \Delta\beta_{s_7} \;\; \Delta\beta_{s_8} \rangle \tag{22}$$

$$[B_{b_u}] = \begin{bmatrix} & 0 & \dfrac{\partial N_i}{\partial x} & 0 & \\ \cdots & 0 & 0 & \dfrac{\partial N_i}{\partial y} & \cdots i = 1,2,3,4 \\ & 0 & \dfrac{\partial N_i}{\partial y} & \dfrac{\partial N_i}{\partial x} & \end{bmatrix}$$

$$\frac{\partial N_i}{\partial x} = j_{11}\frac{\partial N_i}{\partial \xi} + j_{12}\frac{\partial N_i}{\partial \eta}\ ;\ \frac{\partial N_i}{\partial y} = j_{21}\frac{\partial N_i}{\partial \xi} + j_{22}\frac{\partial N_i}{\partial \eta} \tag{23}$$

$$[B_{b_\Delta}] = \begin{bmatrix} & \dfrac{\partial P_k}{\partial x}C_k & \\ \cdots & \dfrac{\partial P_k}{\partial y}S_k & \cdots \quad k = 5,6,7,8 \\ & \dfrac{\partial P_k}{\partial y}C_k + \dfrac{\partial P_k}{\partial x}S_k & \end{bmatrix}$$

$$\frac{\partial P_k}{\partial x} = j_{11}\frac{\partial P_k}{\partial \xi} + j_{12}\frac{\partial P_k}{\partial \eta}\ ;\ \frac{\partial P_k}{\partial y} = j_{21}\frac{\partial P_k}{\partial \xi} + j_{22}\frac{\partial P_k}{\partial \eta}$$

where $[B_{b_u}]$ is the *l*-order bending strains matrix, and $[B_{b_\Delta}]$ is the *h*-order bending strains matrix

The bending energy is expressed as follows:

$$\Pi^b_{int} = \frac{1}{2}\int_A \langle\chi\rangle[H_b]\{\chi\} \tag{24}$$

$[H_b]$ is the constitutive matrix for bending moments (10). Substituting (22) into (24), we get:

$$\Pi^b_{int} = \frac{1}{2}\left\langle u_n \quad | \quad \Delta\beta_{s_n}\right\rangle \begin{bmatrix} [k_{b_u}] & | & [k_{b_{u\Delta}}] \\ [k_{b_{\Delta u}}] & | & [k_{b_\Delta}] \end{bmatrix} \begin{Bmatrix} u_n \\ \Delta\beta_{s_n} \end{Bmatrix}$$

$$[k_{b_u}] = \int_A [B_{b_u}]^T[H_b][B_{b_u}]dA$$

$$[k_{b_\Delta}] = \int_A [B_{b_\Delta}]^T[H_b][B_{b_\Delta}]dA \tag{25}$$

$$[k_{b_{u\Delta}}] = [k_{b_{\Delta u}}]^T = \int_A [B_{b_u}]^T[H_b][B_{b_\Delta}]dA$$

$[k_{b_u}]$, $[k_{b_{u\Delta}}]$, $[k_{b_\Delta}]$ are the *l*-order, *c*-order, and *h*-order bending stiffness, respectively.

In the DSQK element [5], the couple bending energy in (25) is considered spurious, and the assumed orthogonality condition [7,8] is applied, which states that the couple bending stiffness $[k_{b_{u\Delta}}]$ and $[k_{b_{\Delta u}}]$ in (25) are to be zero, and the bending energy in (25) for the DSQK element:

$$\Pi^b_{int} = \frac{1}{2}\langle u_n\rangle[k_{b_u}]\{u_n\} + \frac{1}{2}\langle\Delta\beta_n\rangle[k_{b_\Delta}]\{\Delta\beta_n\} \tag{26}$$

2.7. Transverse shear strains

2.7.1. Kinematic transverse shear strains

The kinematic transverse shear strain along each side is

$$\gamma_s = \frac{\partial w}{\partial s} + \beta_s \tag{27}$$

The quadratic kinematic transverse shear strain on side *k* can be obtained by introducing (19) into (27):

$$\gamma_s = \left(\frac{w_j - w_i}{L_k}\right) + \left(1 - \frac{s}{L_k}\right)\beta_{s_i} + \left(\frac{s}{L_k}\right)\beta_{s_j} + 4\frac{s}{L_k}\left(1 - \frac{s}{L_k}\right)\Delta\beta_{s_k} \tag{28}$$

The constant kinematic transverse shear strain alongside *k* can be obtained using the discrete shear constraint as follows:

$$\underline{\gamma}_{s_k} = \int_s \gamma_s\, ds = \frac{w_j - w_i}{L_k} + \frac{1}{2}\left(C_k\beta_{x_i} + S_k\beta_{y_i} + C_k\beta_{x_j} + S_k\beta_{y_j}\right) + \frac{2}{3}\Delta\beta_{s_k} \tag{29}$$

Applying (29) on four sides of the element, we get:

$$\left\{\underline{\gamma}_{s_n}\right\} = [A_u]\{u_n\} + [A_\Delta]\{\Delta\beta_{s_n}\}$$

$$[A_u] = [\,[A_{u_1}] \quad [A_{u_2}]\,]$$

$$[A_{u_1}] = \begin{bmatrix} -\dfrac{1}{L_5} & \dfrac{C_5}{2} & \dfrac{S_5}{2} & \dfrac{1}{L_5} & \dfrac{C_5}{2} & \dfrac{S_5}{2} \\ 0 & 0 & 0 & -\dfrac{1}{L_6} & \dfrac{C_6}{2} & \dfrac{S_6}{2} \\ 0 & 0 & 0 & 0 & 0 & 0 \\ \dfrac{1}{L_8} & \dfrac{C_8}{2} & \dfrac{S_8}{2} & 0 & 0 & 0 \end{bmatrix}$$

$$[A_{u_2}] = \begin{bmatrix} 0 & 0 & 0 & 0 & 0 & 0 \\ \dfrac{1}{L_6} & \dfrac{C_6}{2} & \dfrac{S_6}{2} & 0 & 0 & 0 \\ -\dfrac{1}{L_7} & \dfrac{C_7}{2} & \dfrac{S_7}{2} & \dfrac{1}{L_7} & \dfrac{C_7}{2} & \dfrac{S_7}{2} \\ 0 & 0 & 0 & -\dfrac{1}{L_6} & \dfrac{C_8}{2} & \dfrac{S_8}{2} \end{bmatrix} \tag{30}$$

$$[A_\Delta] = \frac{2}{3}\begin{bmatrix} 1 & 0 & 0 & 0 \\ 0 & 1 & 0 & 0 \\ 0 & 0 & 1 & 0 \\ 0 & 0 & 0 & 1 \end{bmatrix}$$

2.7.2. The mixed transverse shear strains

The mixed transverse shear strain is obtained by unifying the equations of bending strains (2), kinematic transverse shear strains (3), plate equilibrium (4), constitutive law of bending moments (8), and the constitutive law of shear forces (9). Finally, the mixed transverse shear strains are defined as the second derivatives of the rotation functions:

$$\left\{\underline{\gamma}\right\} = \begin{Bmatrix} \underline{\gamma}_x \\ \underline{\gamma}_y \end{Bmatrix} = \frac{D_b}{D_s}\begin{Bmatrix} \dfrac{\partial^2\beta_x}{\partial x^2} + \left(\dfrac{1-\upsilon}{2}\right)\dfrac{\partial^2\beta_x}{\partial y^2} + \left(\dfrac{1+\upsilon}{2}\right)\dfrac{\partial^2\beta_y}{\partial x\partial y} \\ \dfrac{\partial^2\beta_y}{\partial y^2} + \left(\dfrac{1-\upsilon}{2}\right)\dfrac{\partial^2\beta_y}{\partial x^2} + \left(\dfrac{1+\upsilon}{2}\right)\dfrac{\partial^2\beta_x}{\partial x\partial y} \end{Bmatrix} \tag{31a}$$

Substituting (20) into (31a) leads to:

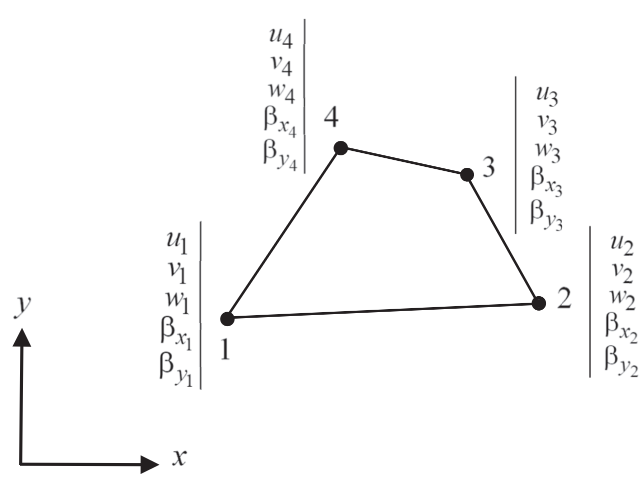

Fig. 7. DSQK plate element with final 5 DOFs per node.

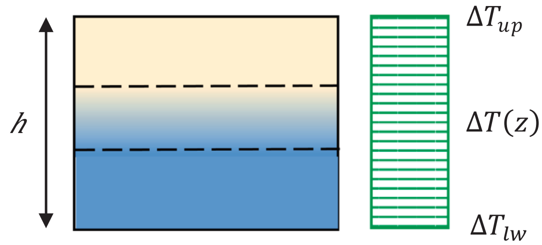

Fig. 8. Uniform temperature rise.

$$
\begin{gathered}
\left\{\underline{\gamma}\right\} = \begin{Bmatrix} \gamma_x \\ \gamma_y \end{Bmatrix} = [B_{s_\Delta}]\{\Delta\beta_{s_n}\} \\
[B_{s_\Delta}(\xi,\eta)] = [\underline{H}_s][T_j(\xi,\eta)][T_\Delta(\xi,\eta)] \\
[\underline{H}_s] = \frac{D_b}{D_s}\begin{bmatrix} 1 & \frac{(1-\upsilon)}{2} & 0 & 0 & 0 & \frac{(1+\upsilon)}{2} \\ 0 & 0 & \frac{(1+\upsilon)}{2} & \frac{(1-\upsilon)}{2} & 1 & 0 \end{bmatrix} \\
[T_j(\xi,\eta)] = \begin{bmatrix} [t_j] & [0] \\ [0] & [t_j] \end{bmatrix} \\
[t_j] = \begin{bmatrix} j_{11}^2 & j_{12}^2 & 2j_{11}j_{12} \\ j_{21}^2 & j_{22}^2 & 2j_{21}j_{22} \\ j_{11}j_{21} & j_{12}j_{22} & j_{11}j_{22}+j_{12}j_{21} \end{bmatrix} \\
[T_\Delta] = \begin{bmatrix} -C_5(1-\eta) & 0 & -C_7(1+\eta) & 0 \\ 0 & -C_6(1+\xi) & 0 & -C_8(1-\xi) \\ C_5\xi & -C_6\eta & -C_7\xi & C_8\eta \\ -S_5(1-\eta) & 0 & -S_7(1+\eta) & 0 \\ 0 & -S_6(1+\xi) & 0 & -S_8(1-\xi) \\ S_5\xi & -S_6\eta & -S_7\xi & S_8\eta \end{bmatrix}
\end{gathered}
\tag{31b}
$$

The collocation method is applied to obtain the constant value of mixed transverse shear strain on sides k ($k = 5, 8$):

$$
\underline{\gamma}_{s_k} = \langle C_k \quad S_k \rangle \begin{Bmatrix} \underline{\gamma}_x(\xi_k,\eta_k) \\ \underline{\gamma}_y(\xi_k,\eta_k) \end{Bmatrix} = \langle C_k \quad S_k \rangle [B_{s_\Delta}(\xi_k,\eta_k)]\{\Delta\beta_{s_n}\}
\tag{32}
$$

Applying (32) on four sides of the element, we get:

$$
\begin{gathered}
\left\{\underline{\gamma}_{s_n}\right\} = [A_\gamma]\{\Delta\beta_{s_n}\} \\
[A_\gamma] = \begin{bmatrix} \langle C_5 \quad S_5 \rangle [B_{s_\Delta}(\xi_5 = 0, \eta_5 = -1)] \\ \langle C_6 \quad S_6 \rangle [B_{s_\Delta}(\xi_6 = +1, \eta_6 = 0)] \\ \langle C_7 \quad S_7 \rangle [B_{s_\Delta}(\xi_7 = 0, \eta_7 = +1)] \\ \langle C_8 \quad S_8 \rangle [B_{s_\Delta}(\xi_8 = -1, \eta_8 = 0)] \end{bmatrix}
\end{gathered}
\tag{33}
$$

2.7.3. Elimination of temporary DOFs

To obtain good bending behaviour, the quadrilateral DSQK element is formulated using temporary DOFs, which play the role of enhancing the rotation function (20) to be quadratic. These temporary DOFs $\langle \Delta\beta_{s_n} \rangle$ are then removed by equalising (30) and (33). We get:

$$
\begin{gathered}
[A_u]\{u_n\} + [A_\Delta]\{\Delta\beta_{s_n}\} = [A_\gamma]\{\Delta\beta_{s_n}\} \\
\{\Delta\beta_{s_n}\} = [A_n]\{u_n\} \; ; \; [A_n] = [[A_\gamma] - [A_\Delta]]^{-1}[A_u]
\end{gathered}
\tag{34}
$$

2.8. Bending stiffness

Introducing Eq. (34) into Eq. (22) leads to

$$
\begin{gathered}
\{\chi\} = [B_b]\{u_n\} \\
[B_b] = [B_{b_u}] + [B_{b_\Delta}][A_n]
\end{gathered}
\tag{35}
$$

Introducing (35) into (24), the bending energy and stiffness for DSQ [6] become:

$$
\begin{aligned}
\Pi_{int}^b &= \frac{1}{2}\langle u_n \rangle [k_b]\{u_n\} \\
[k_b] &= \int_A [B_b]^T [H_b][B_b] dA
\end{aligned}
\tag{36}
$$

Introducing (34) into (26), the bending strain energy and stiffness for DSQK [5] finally become:

$$
\begin{aligned}
\Pi_{int}^b &= \frac{1}{2}\langle u_n \rangle [k_b]\{u_n\} \\
[k_b] &= [k_{b_u}] + [A_n]^T [k_{b_\Delta}][A_n]
\end{aligned}
\tag{37}
$$

2.9. Membrane-bending stiffness

The couple energy of membrane-bending stiffness is given by:

$$
\begin{gathered}
\Pi_{int}^{mb} = \frac{1}{2}\int_A \langle e \rangle [H_{mb}]\{\chi\} dA + \frac{1}{2}\int_A \langle \chi \rangle [H_{mb}]\{e\} dA \\
\Pi_{int}^{mb} = \frac{1}{2}\langle u_n \rangle ([k_{mb}] + [k_{mb}]^T)\{u_n\} \\
[k_{mb}] = \int_A [B_m]^T [H_{mb}][B_b] dA
\end{gathered}
\tag{38}
$$

$[H_{mb}]$ is the constitutive matrix for a couple of membrane-bending strains in FGM plates (10).

2.10. Transverse shear stiffness

Introducing Eq. (34) into Eq. (31), we obtain for DSQ [6] and DSQK [5]:

$$
\begin{gathered}
\left\{\underline{\gamma}\right\} = [B_s]\{u_n\} \\
[B_s] = [B_{s_\Delta}][A_n]
\end{gathered}
\tag{39}
$$

The transverse shear strain energy and stiffness:

$$
\begin{gathered}
\Pi_{int}^s = \frac{1}{2}\int_A \left\langle \underline{\gamma} \right\rangle [H_s]\left\{\underline{\gamma}\right\} dA = \frac{1}{2}\langle u_n \rangle [k_s]\{u_n\} \\
[k_s] = \int_A [B_s]^T [H_s][B_s] dA
\end{gathered}
\tag{40}
$$

$[H_s]$ is the constitutive matrix for shear forces (10).

2.11. Total stiffness

The final stiffness of DSQ and DSQK elements for the FGM sandwich plate is:

$$
[k] = [k_m] + [k_b] + [k_{mb}] + [k_{mb}]^T + [k_s]
\tag{41}
$$

Equations (35) to (40) no longer contain temporary DOFs $\{\Delta\beta_n\}$, so $\{u_n\}$ (17) is the final DOFs for the DSQ and DSQK elements, as can be seen in Fig. 7.

2.12. Thermal buckling analysis

For thermal buckling analysis, it is common to adopt the so-called von Kármán kinematic model, assuming that for a flat plate, the buckling mode is characterised by the Green-Lagrange strain tensor, which considers only second-order terms related to the out-of-plane displacement w.

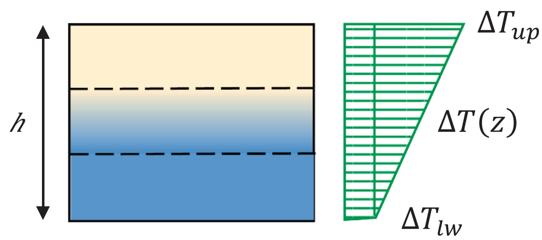

Fig. 9. Linear temperature rise.

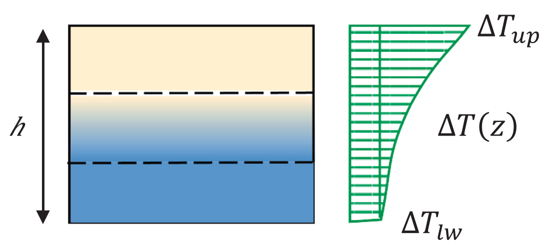

Fig. 10. Nonlinear temperature rise.

$$\{\varepsilon\} = \begin{Bmatrix} \varepsilon_x \\ \varepsilon_y \\ \gamma_{xy} \end{Bmatrix} = z \begin{Bmatrix} \chi_x \\ \chi_y \\ \chi_{xy} \end{Bmatrix} + \begin{Bmatrix} \frac{1}{2}\frac{\partial^2 w}{\partial x^2} \\ \frac{1}{2}\frac{\partial^2 w}{\partial y^2} \\ \frac{\partial w}{\partial x}\frac{\partial w}{\partial y} \end{Bmatrix} \tag{42}$$

The membrane strain energy associated with the von Kármán model is defined as follows:

$$\Pi_{int}^{\sigma} = \frac{1}{2}\int_A \langle \nabla w \rangle [\sigma^0] \{\nabla w\} h\, dA; \ \{\nabla w\} = [G_w]\{u_n\}$$
$$\Pi_{int}^{\sigma} = \frac{1}{2}\langle u_n \rangle [k_G]\{u_n\} \tag{43}$$

$$[k_G] = h\int_A [G_w]^T [\sigma^0] [G_w] dA$$
$$[G_w] = \begin{bmatrix} \cdots & 0 & 0 & \frac{\partial N_i}{\partial x} & 0 & 0 & \cdots \\ & 0 & 0 & \frac{\partial N_i}{\partial y} & 0 & 0 & \end{bmatrix}_{i=1-3} \tag{44}$$

In function of normal forces, we have

$$[\sigma^0] = \frac{N_{cr}}{h}\begin{bmatrix} 1 & 0 \\ 0 & 1 \end{bmatrix} \tag{45}$$

While for thermal load:

$$N_{cr} = \frac{1}{(1-\upsilon)}\sum_{n=1}^{3}\int_{h_{n-1}}^{h_n} E^n(z)\alpha^n(z)\Delta T(z) dz \tag{46}$$

$E^n(z)$ and $\alpha^n(z)$ are defined in (5). In linear buckling analysis, the eigenvalue problem is expressed as:

$$([k] - N_{cr}[k_G])\{u_n\} = \{0\} \tag{47}$$

where N_{cr} is the buckling load parameter.

The studies in this paper dealt with the thermal buckling behaviour due to constant, linear, and nonlinear temperature distributions across the thickness. Let's consider a rectangular plate with upper and lower surface temperature changes ΔT_{up} and ΔT_{lw}, respectively.

In uniform temperature rise (UTR) (Fig. 8):

$$\Delta T(z) = \Delta T_{cr} = \Delta T_{up} = \Delta T_{lw} \tag{48}$$

From (46), we obtain,

$$N_{cr} = D_T^U \Delta T_{cr}$$
$$D_T^U = \frac{1}{(1-\upsilon)}\sum_{n=1}^{3}\int_{h_{n-1}}^{h_n} E^n(z)\alpha^n(z) dz \tag{49}$$
$$\Delta T(z) = \Delta T_{cr}$$

The UTR critical buckling temperature change:

$$\Delta T_{cr} = \frac{N_{cr}}{D_T^U} \tag{50}$$

In the linear temperature rise (LTR), the temperature as a function of z (Fig. 9) is as follows:

$$\Delta T(z) = \Delta T_{lw} + \Delta T_{cr}\left(\frac{1}{2} + \frac{z}{h}\right) \ ; \ \Delta T_{cr} = \Delta T_{up} - \Delta T_{lw} \tag{51}$$

From (46), we have

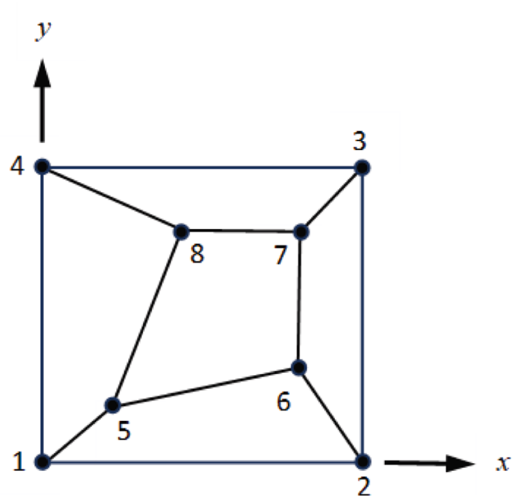

Node	x	y
1	0	0
2	10	0
3	10	10
4	0	10
5	2	2
6	8	3
7	8	7
8	4	7

Fig. 11. Constant curvature patch-test with 5 elements.

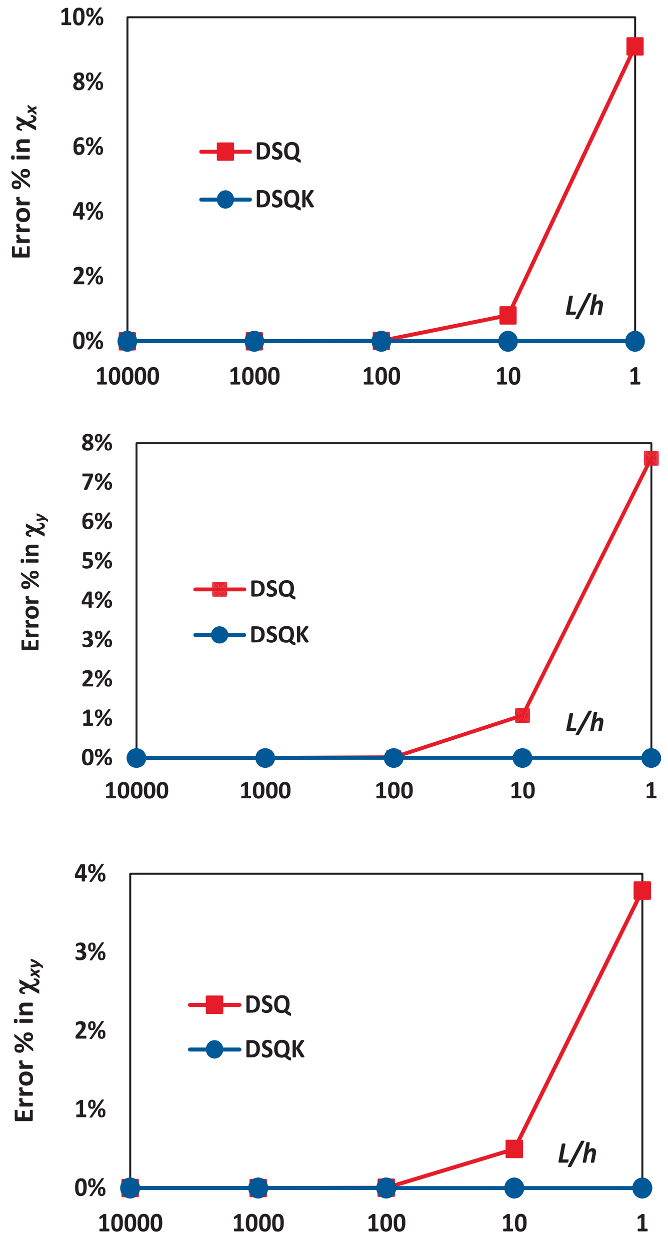

Fig. 12. Kinematical constant curvature patch test, the effect of L/h using DSQ and DSQK.

Table 1
Internal energies $2\Pi_{int}$ of clamped circular plates.

	$2\Pi_{int}^{FE} = 10^3 \times 2\Pi_{int}^{FE} \times D_b/f_z^2R^6$					
	$2R/h = 1000$			$2R/h = 5$		
N	DSQK [5]	DSQ [6]	BWQ [7]	DSQK [5]	DSQ [6]	BWQ [7]
4	4.182	4.012	4.155	8.601	8.530	8.571
8	4.114	4.099	4.107	8.584	8.566	8.582
16	4.097	4.093	4.095	8.580	8.575	8.581
32	4.092	4.091	4.092	8.579	8.578	8.579
64	4.091	4.091	4.091	8.579	8.578	8.579
128	4.091	4.091	4.091	8.579	8.578	8.579
Exact	4.091			8.579		

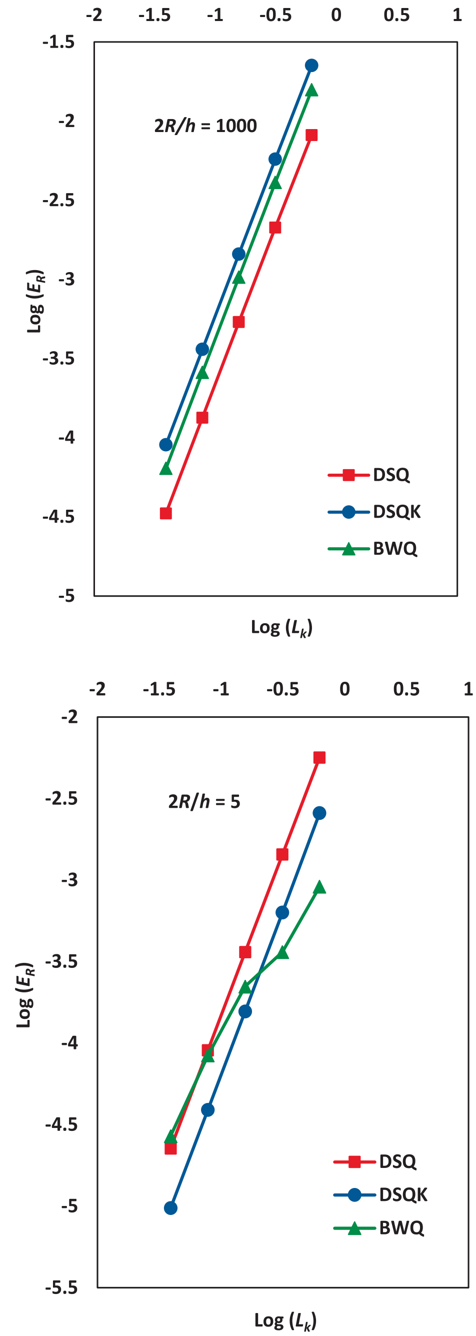

Fig. 13. Convergence behaviour of fully clamped circular plates using Log (|E_R|) versus Log (L_k).

$$N_{cr} = \Delta T_{lw} D_T^U + \Delta T_{cr} D_T^L$$

$$D_T^U = \frac{1}{(1-\upsilon)} \sum_{n=1}^{3} \int_{h_{n-1}}^{h_n} E^n(z)\, \alpha^n(z)\, dz \tag{52}$$

$$D_T^L = \frac{1}{(1-\upsilon)} \sum_{n=1}^{3} \int_{h_{n-1}}^{h_n} E^n(z)\, \alpha^n(z) \left(\frac{1}{2} + \frac{z}{h}\right) dz$$

The LTR critical buckling temperature change (Fig. 9) is:

$$\Delta T_{cr} = \frac{N_{cr} - \Delta T_{lw} D_T^U}{D_T^L} \tag{53}$$

In the nonlinear temperature rise (NLTR) (Fig. 10), the equation of the steady-state heat transfer at the interfaces is expressed as:

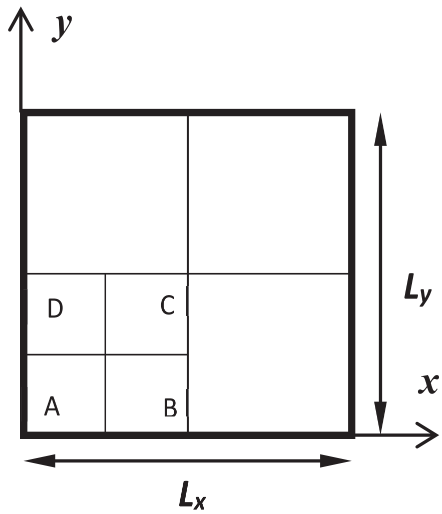

Fig. 14. 1/4 square plate model.

$$-\frac{d}{dz}\left(K^{n}(z)\frac{dT}{dz}\right)=0 \tag{54}$$

K^{n} (z) is the coefficient of thermal conductivity and varies continuously across the FGM in the n-layer (5). The temperature variation through the plate thickness is expressed as

$$\Delta T(z)=\Delta T_{lw}+\Delta T_{cr}\Theta(z)\ ;\ \Delta T_{cr}=\Delta T_{up}-\Delta T_{lw} \tag{55}$$

$$\begin{aligned}
&h_0\leqslant z\leqslant h_1:\Theta^{(1)}(z)=\frac{\int_{h_0}^{z}\frac{1}{K^{(1)}(z)}dz}{\sum_{n=1}^{3}\int_{h_{n-1}}^{h_n}\frac{1}{K^{(n)}(z)}dz}\\
&h_1\leqslant z\leqslant h_2:\Theta^{(2)}(z)=\frac{\int_{h_0}^{h_1}\frac{1}{K^{(1)}(z)}dz+\int_{h_1}^{z}\frac{1}{K^{(2)}(z)}dz}{\sum_{n=1}^{3}\int_{h_{n-1}}^{h_n}\frac{1}{K^{(n)}(z)}dz}\\
&h_2\leqslant z\leqslant h_3:\Theta^{(3)}(z)=\frac{\int_{h_0}^{h_1}\frac{1}{K^{(1)}(z)}dz+\int_{h_1}^{h_2}\frac{1}{K^{(2)}(z)}dz+\int_{h_2}^{z}\frac{1}{K^{(3)}(z)}dz}{\sum_{n=1}^{3}\int_{h_{n-1}}^{h_n}\frac{1}{K^{(n)}(z)}dz}
\end{aligned} \tag{56}$$

From (46), we obtain

$$\begin{aligned}
&N_{cr}=\Delta T_{lw}D_T^{U}+\Delta T_{cr}D_T^{NL}\\
&D_T^{U}=\frac{1}{(1-\upsilon)}\sum_{n=1}^{3}\int_{h_{n-1}}^{h_n}E^{n}(z)\,\alpha^{n}(z)\ dz\\
&D_T^{NL}=\frac{1}{(1-\upsilon)}\sum_{n=1}^{3}\int_{h_{n-1}}^{h_n}E^{n}(z)\,\alpha^{n}(z)\Theta(z)dz
\end{aligned} \tag{57}$$

The critical buckling temperature (CBT) change for NLTR is

$$\Delta T_{cr}=\frac{N_{cr}-\Delta T_{lw}D_T^{U}}{D_T^{NL}} \tag{58}$$

3. Validation and numerical analysis

The numerical analysis in this study utilised an in-house FE code developed in MATLAB, and the eigenvalues were solved using the standard libraries available in MATLAB. All the numerical studies employed a uniform mesh.

Table 2
ΔT_{cr} (∘C) of square FG sandwich plates under UTR for various L/h.

Scheme	p	L/h	DSQK 4 × 4	DSQK 8 × 8	DSQK 16 × 16	Q4γ_s [55]	FSDT [56]	HSDT [56]
1-1-1		5	2.67514	2.66630	2.66414	2.66649	2.66342	2.68634
		10	0.75066	0.74775	0.74706	0.74780	0.74683	0.74857
	0.5	15	0.34142	0.34001	0.33968	0.34003	0.33957	0.33993
		25	0.12442	0.12387	0.12375	0.12387	0.12370	0.12375
		50	0.03127	0.03113	0.03109	0.03113	0.03108	0.03108
		5	2.88077	2.86829	2.86523	2.86748	2.86421	2.85194
		10	0.81451	0.81039	0.80940	0.81011	0.80907	0.80801
	2	15	0.37107	0.36907	0.36860	0.36894	0.36845	0.36822
		25	0.13535	0.13457	0.13439	0.13452	0.13433	0.13430
		50	0.03403	0.03383	0.03378	0.03381	0.03376	0.03376
1-2-1		5	2.73860	2.73228	2.73075	2.73338	2.73024	2.75276
		10	0.77047	0.76835	0.76786	0.76869	0.76769	0.76941
	0.5	15	0.35062	0.34958	0.34934	0.34973	0.34926	0.34961
		25	0.12781	0.12740	0.12730	0.12745	0.12727	0.12732
		50	0.03213	0.03202	0.03199	0.03203	0.03198	0.03198
		5	3.01369	3.00181	2.99889	3.00132	2.99792	2.97362
		10	0.85600	0.85203	0.85108	0.85186	0.85076	0.84870
	2	15	0.39035	0.38842	0.38797	0.38833	0.38782	0.38739
		25	0.14245	0.14170	0.14153	0.14166	0.14147	0.14141
		50	0.03583	0.03563	0.03558	0.03562	0.03556	0.03556
2-2-1		5	2.85377	2.84272	2.84001	2.84236	2.83911	2.84152
		10	0.80570	0.80205	0.80118	0.80192	0.80088	0.80101
	0.5	15	0.36694	0.36517	0.36475	0.36510	0.36461	0.36464
		25	0.13382	0.13313	0.13297	0.13310	0.13291	0.13292
		50	0.03364	0.03346	0.03342	0.03345	0.03340	0.03340
		5	3.28816	3.27551	3.27240	3.27503	3.27137	3.19501
		10	0.94367	0.93936	0.93833	0.93919	0.93798	0.93147
	2	15	0.43129	0.42919	0.42870	0.42911	0.42854	0.42717
		25	0.15758	0.15676	0.15658	0.15672	0.15651	0.15633
		50	0.03965	0.03944	0.03939	0.03942	0.03937	0.03935

Table 3
ΔT_{cr} (∘C) of square FG sandwich plates under LTR for various L/h.

Scheme	p	L/h	DSQK 4 × 4	DSQK 8 × 8	DSQK 16 × 16	Q4γ_s [55]	FSDT [56]	HSDT [56]
1-1-1		5	4.11516	4.10143	4.09808	4.10173	4.09696	4.13256
		10	1.12682	1.12230	1.12123	1.12238	1.12087	1.12357
	0.5	15	0.49135	0.48915	0.48864	0.48917	0.48847	0.48903
		25	0.15439	0.15353	0.15333	0.15353	0.15327	0.15334
		50	0.00974	0.00952	0.00946	0.00951	0.00944	0.00945
		5	4.27778	4.25909	4.25450	4.25787	4.25298	4.23460
		10	1.18264	1.17646	1.17498	1.17606	1.17449	1.17290
	2	15	0.51839	0.51540	0.51470	0.51520	0.51447	0.51413
		25	0.16529	0.16414	0.16387	0.16405	0.16378	0.16373
		50	0.01353	0.01323	0.01315	0.01320	0.01313	0.01312
1-2-1		5	4.30002	4.28999	4.28757	4.29173	4.28676	4.32245
		10	1.18128	1.17793	1.17714	1.17846	1.17688	1.17961
	0.5	15	0.51598	0.51433	0.51396	0.51457	0.51383	0.51439
		25	0.16291	0.16226	0.16211	0.16234	0.16206	0.16214
		50	0.01129	0.01112	0.01108	0.01114	0.01106	0.01107
		5	4.48551	4.46767	4.46330	4.46694	4.46184	4.42537
		10	1.24718	1.24122	1.23980	1.24097	1.23932	1.23623
	2	15	0.54832	0.54543	0.54475	0.54530	0.54453	0.54388
		25	0.17628	0.17515	0.17489	0.17509	0.17480	0.17472
		50	0.01625	0.01595	0.01588	0.01593	0.01586	0.01585
2-2-1		5	4.29406	4.27728	4.27317	4.27673	4.27180	4.27547
		10	1.18511	1.17956	1.17823	1.17936	1.17779	1.17798
	0.5	15	0.51906	0.51637	0.51574	0.51627	0.51553	0.51557
		25	0.16518	0.16414	0.16390	0.16409	0.16382	0.16382
		50	0.01312	0.01285	0.01278	0.01283	0.01276	0.01276
		5	4.83907	4.82031	4.81570	4.81959	4.81417	4.70093
		10	1.36233	1.35594	1.35441	1.35569	1.35390	1.34424
	2	15	0.60251	0.59939	0.59866	0.59926	0.59842	0.59639
		25	0.19661	0.19540	0.19512	0.19534	0.19503	0.19475
		50	0.02173	0.02141	0.02133	0.02139	0.02131	0.02129

Table 4
ΔT_{cr} (∘C) of square FG sandwich plates under **N**LTR for various L/h.

Scheme	p	L/h	DSQK 4 × 4	DSQK 8 × 8	DSQK 16 × 16	Q4γ_s [55]	FSDT [56]	HSDT [56]
1-1-1		5	6.65338	6.63118	6.62576	6.63167	6.62363	6.68117
		10	1.82183	1.81453	1.81280	1.81465	1.81213	1.81650
	0.5	15	0.79441	0.79085	0.79003	0.79090	0.78972	0.79062
		25	0.24961	0.24823	0.24791	0.24823	0.24779	0.24791
		50	0.01575	0.01538	0.01530	0.01538	0.01527	0.01527
		5	7.05442	7.02361	7.01604	7.02159	7.01338	6.98307
		10	1.95028	1.94009	1.93765	1.93942	1.93680	1.93418
	2	15	0.85487	0.84994	0.84878	0.84961	0.84838	0.84783
		25	0.27258	0.27067	0.27023	0.27053	0.27008	0.27001
		50	0.02231	0.02181	0.02169	0.02177	0.02165	0.02165
1-2-1		5	7.09285	7.07632	7.07232	7.07919	7.07091	6.76137
		10	1.94852	1.94298	1.94169	1.94386	1.94124	1.94573
	0.5	15	0.85111	0.84838	0.84777	0.84878	0.84756	0.84848
		25	0.26873	0.26765	0.26741	0.26778	0.26732	0.26745
		50	0.01863	0.01834	0.01828	0.01837	0.01825	0.01826
		5	7.73394	7.70319	7.69564	7.70192	7.69300	7.63012
		10	2.15040	2.14012	2.13766	2.13969	2.13681	2.13149
	2	15	0.94542	0.94044	0.93927	0.94021	0.93887	0.93775
		25	0.30394	0.30200	0.30155	0.30190	0.30140	0.30125
		50	0.02802	0.02751	0.02739	0.02747	0.02734	0.02733
2-2-1		5	7.36209	7.33333	7.32628	7.33238	7.32400	7.33028
		10	2.03184	2.02233	2.02006	2.02200	2.01932	2.01965
	0.5	15	0.88992	0.88531	0.88423	0.88514	0.88389	0.88395
		25	0.28321	0.28141	0.28100	0.28133	0.28087	0.28087
		50	0.02250	0.02203	0.02192	0.02200	0.02188	0.02188
		5	8.43039	8.39771	8.38968	8.39646	8.38695	8.18967
		10	2.37338	2.36225	2.35958	2.36181	2.35868	2.34185
	2	15	1.04966	1.04424	1.04296	1.04401	1.04254	1.03900
		25	0.34253	0.34042	0.33993	0.34031	0.33976	0.33929
		50	0.03786	0.03730	0.03717	0.03726	0.03712	0.03709

Table 5
ΔT_{cr} (∘C) of FG sandwich plates under UTR for various $n = L_x/L_y$.

Scheme	n	DSQK $4n \times 4$	DSQK $8n \times 8$	DSQK $16n \times 16$	Q4γ_s [55]	FSDT [56]	HSDT [56]
	1/2	0.55889	0.52497	0.51657	0.51655	0.51401	0.51358
	1	0.83676	0.81605	0.81082	0.81011	0.80907	0.80801
1-1-1	2	1.93580	1.90713	1.89987	1.90147	1.89931	1.89370
	3	3.49714	3.45550	3.44501	3.45209	3.44812	3.43082
	5	6.98304	6.92435	6.90959	6.92808	6.92142	6.86679
	1/2	0.58704	0.55216	0.54352	0.54353	0.54086	0.54002
	1	0.87907	0.85790	0.85256	0.85186	0.85076	0.84870
1-2-1	2	2.02979	2.00046	1.99304	1.99454	1.99229	1.98128
	3	3.65501	3.61257	3.60187	3.60849	3.60437	3.56982
	5	7.24301	7.18393	7.16907	7.18602	7.17921	7.05975
	1/2	0.64793	0.60962	0.60011	0.60014	0.59720	0.59455
	1	0.96898	0.94580	0.93995	0.93919	0.93798	0.93147
2-2-1	2	2.22509	2.19332	2.18529	2.18695	2.18451	2.14984
	3	3.97570	3.93043	3.91902	3.92618	3.92177	3.81326
	5	7.74631	7.68537	7.67005	7.68764	7.68061	7.29624

Table 6
ΔT_{cr} (∘C) of FG sandwich plates under LTR for various $n = L_x/L_y$.

Scheme	n	DSQK $4n \times 4$	DSQK $8n \times 8$	DSQK $16n \times 16$	Q4γ_s [55]	FSDT [56]	HSDT [56]
	1/2	0.76407	0.74007	0.73438	0.73632	0.73251	0.73187
	1	1.18264	1.17646	1.17498	1.17606	1.17449	1.17290
1-1-1	2	2.83317	2.81395	2.80920	2.81084	2.80761	2.79920
	3	5.18165	5.14107	5.13100	5.13360	5.1276	5.10173
	5	10.42681	10.35447	10.33646	10.34044	10.33046	10.24863
	1/2	0.80642	0.78193	0.77612	0.77822	0.77422	0.77296
	1	1.24718	1.24122	1.23980	1.24097	1.23932	1.23623
1-2-1	2	2.97849	2.95899	2.95417	2.95594	2.95256	2.93605
	3	5.42711	5.38571	5.37544	5.37820	5.37201	5.32017
	5	10.83453	10.76149	10.74330	10.74745	10.73724	10.55795
	1/2	0.88344	0.85690	0.85061	0.85290	0.84855	0.84461
	1	1.36233	1.35594	1.35441	1.35569	1.35390	1.34424
2-2-1	2	3.23014	3.20930	3.20414	3.20605	3.20242	3.15102
	3	5.83677	5.79312	5.78229	5.78522	5.77868	5.61776
	5	11.45203	11.37755	11.35899	11.36324	11.35281	10.78282

Table 7
ΔT_{cr} (∘C) of FG sandwich plates under NLTR for various $n = L_x/L_y$.

Scheme	n	DSQK $4n \times 4$	DSQK $8n \times 8$	DSQK $16n \times 16$	Q4γ_s [55]	FSDT [56]	HSDT [56]
	1/2	1.26002	1.22044	1.21105	1.21425	1.20796	1.20689
	1	1.95028	1.94009	1.93765	1.93942	1.93680	1.93418
1-1-1	2	4.67214	4.64044	4.63260	4.63532	4.62990	4.61603
	3	8.54498	8.47805	8.46145	8.46573	8.45574	8.41301
	5	17.19469	17.07540	17.04570	17.05225	17.03545	16.90051
	1/2	1.39044	1.34820	1.33819	1.34181	1.33489	1.33272
	1	2.15040	2.14012	2.13766	2.13969	2.13681	2.13149
1-2-1	2	5.13552	5.10191	5.09359	5.09665	5.09074	5.06226
	3	9.35745	9.28607	9.26836	9.27313	9.26230	9.17291
	5	18.68095	18.55502	18.52366	18.53081	18.51289	18.20376
	1/2	1.53908	1.49285	1.48189	1.48588	1.47829	1.47143
	1	2.37338	2.36225	2.35958	2.36181	2.35868	2.34185
2-2-1	2	5.62740	5.59108	5.58210	5.58542	5.57906	5.48951
	3	10.16853	10.09250	10.07362	10.07872	10.06725	9.78692
	5	19.95116	19.82141	19.78908	19.79648	19.77815	18.78516

3.1. Kinematic patch tests

A constant curvature (pure bending) state is used to validate the DSQK element. It is defined as follows:

$$w = -\frac{1}{2}\left(x^2 + y^2 + xy\right)$$
$$\beta_x = x + \frac{1}{2}y \; ; \; \beta_y = y + \frac{1}{2}x \tag{59}$$

Let us consider a rectangular domain with length $L = 10$ as in Fig. 11 ($E = 1000$; $\upsilon = 0.3$; $\kappa = 5/6$). The values of w, β_x, and β_y are imposed at nodes 1, 2, 3, and 4 according to Eq. (59). The values of w, β_x, and β_y at the interior nodes 5–8 are computed using the DSQK [5] and the DSQ [6].

In Fig. 12, it is found that the DSQK element fully satisfies the kinematic patch-tests for any L/h, i.e., the values of w_i, β_{xi}, and β_{yi}: $i = 5, 6, 7, 8$ are in accordance with (59), $\chi_x = \chi_y = \chi_{xy} = 1$, and the shear strains $\gamma_x = \gamma_y = 0$. However, for the DSQ element, the constant curvature patch test is not fully satisfied when $L/h < 100$, indicating the presence of spurious bending energy.

3.2. Errors in energy norm

Error in strain energy for a particular element with different meshes

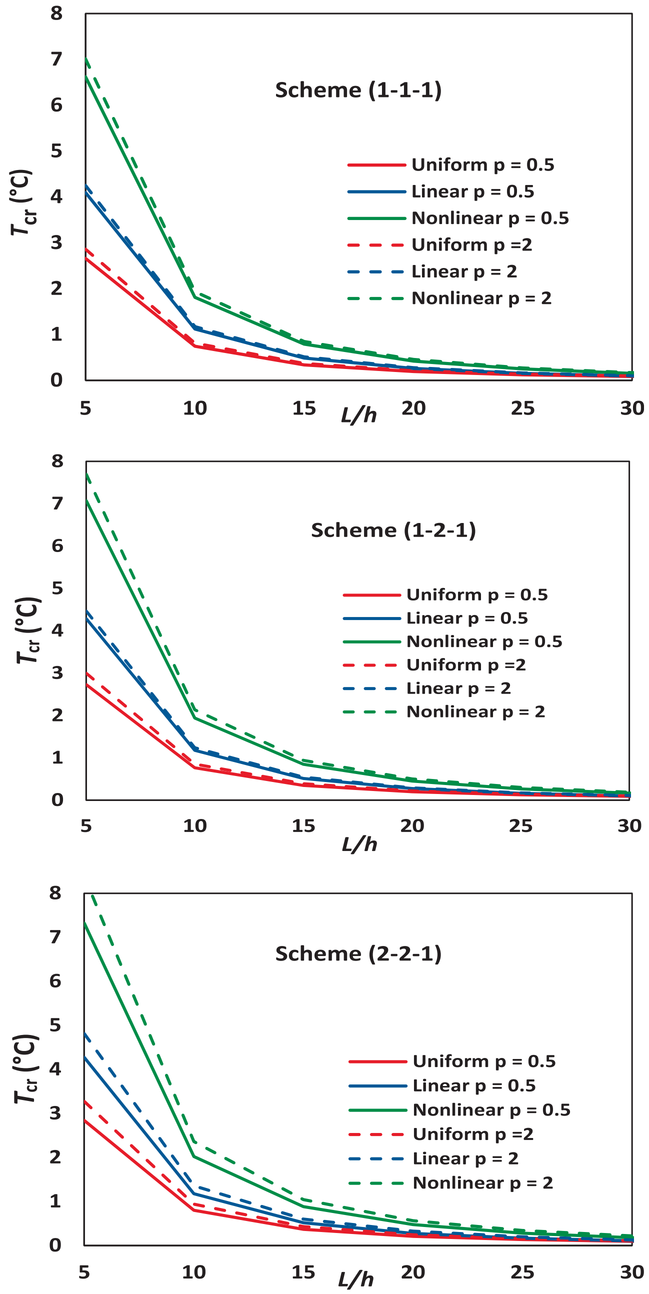

Fig. 15. ΔT_{cr} as a function of the length-thickness ratio L/h for a simply-supported square FGM sandwich plate under UTR, LTR, and NLTR temperature loading using DSQK element.

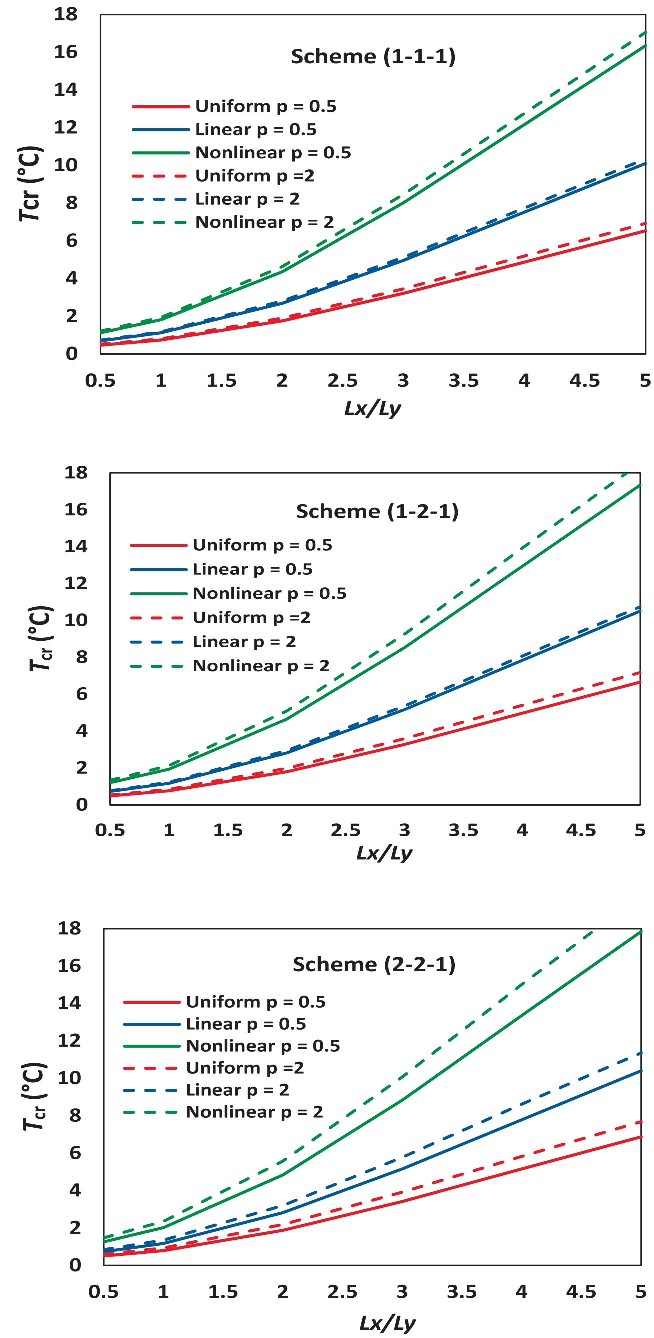

Fig. 16. ΔT_{cr} as a function of the length-side ratio L_x/L_y for a simply-supported rectangular FGM sandwich plate under UTR, LTR, and NLTR temperature loading ($L_x/h = 10$) using DSQK element.

can give an interesting indication of the behaviour and convergence characteristics of the element. The errors in norm energy are defined in (60–64) when an exact solution is available (circular plates). Numerical tests based on the relative errors in the energy norm defined below:

$$E_R = \frac{\|e^{\mathrm{FE}}\|^2}{\|\Pi_{\mathrm{int}}^{\mathrm{Ex}}\|^2} = \frac{\|\Pi_{\mathrm{int}}^{\mathrm{Ex}}\|^2 - \|\Pi_{\mathrm{int}}^{\mathrm{FE}}\|^2}{\|\Pi_{\mathrm{int}}^{\mathrm{Ex}}\|^2} \tag{60}$$

where:

- $\|\Pi_{\mathrm{int}}^{\mathrm{Ex}}\|^2$: the analytical solution of the strain energy.
- $\|\Pi_{\mathrm{int}}^{\mathrm{FE}}\|^2$: the result of the finite element model.

$$\|\Pi_{\mathrm{int}}^{\mathrm{FE}}\|^2 = \sum_{1}^{NELT} \|\Pi_{\mathrm{int}}^{\mathrm{FE}}\|_e^2 \tag{61}$$

$$\|\Pi_{\mathrm{int}}^{\mathrm{FE}}\|_e^2 = \frac{1}{2}\int_A \langle u_n \rangle [k] \{u_n\}\, dA \tag{62}$$

The analytical expression of the strain energy for a simply supported circular plate is:

$$2\Pi_{\mathrm{int}}^{\mathrm{EX}} = \frac{f_z^2 R^6 \varphi}{384 D_b}\left(\left(\frac{7+\upsilon}{1+\upsilon}\right) + \frac{4}{\kappa(1-\upsilon)}\left(\frac{h}{R}\right)^2\right) \tag{63}$$

$\varphi = \pi/2$ is a one quarter of circular plates

The analytical expression of the strain energy for a clamped circular plate is:

$$2\Pi_{\text{int}} = \frac{f_z^2 R^6 \varphi}{384 D_b}\left(1 + \frac{4}{\kappa(1-\upsilon)}\left(\frac{h}{R}\right)^2\right) \tag{64}$$

$\varphi = \pi/2$ is a one quarter ABC

The results of dimensionless internal energies of clamped circular plates are presented in Table 1.

The second-order convergence of the energy norm is expected from the DSQK element. Fig. 13 presents the error in the energy norm (60–64) in log (E_R) and log L_k with L_k the element side length for $N = 4$, 8, 16, 32, and 64. A uniform linear convergence rate for DSQK [5] and DSQ [6] for $2R/h = 1000$ and $2R/h = 5$ is observed for clamped boundary conditions with gradient 2. We also report the results using the BWQ [7] element with linear convergence in thin ($2R/h = 1000$) but nonlinear convergence for thick plates ($2R/h = 5$).

3.3. FGM sandwich plates

For the various schemes of FGM sandwich plates, parametric studies are conducted to show the accuracy of the DSQK formulation discussed in the previous sections. Let us analyze the three-layer FGM rectangular plates $L_x \times L_y \times h$ (Fig. 14). For square plates, $L = L_x = L_y$ and $L_x/L_y = 1$.

To illustrate the proposed DSQK element formulation under thermal buckling load, a metal-ceramic FGM sandwich rectangular plate is considered. The mixture of materials consists of Ti-Al_6-4 V (titanium alloy) and ZrO_2 (zirconia). To simplify, $\upsilon = 0.3$ and $\kappa = 5/6$ are constant for metal and ceramic.

Three different schemes are studied:

1-1-1: the three equal layers ($h_1 = -h/6$; $h_2 = +h/6$).

1-2-1: the core layer equals the sum of the upper and lower layers ($h_1 = -h/4$; $h_2 = +h/4$).

2-2-1: the core and lower layer are twice the upper layer ($h_1 = -h/10$; $h_2 = +3h/10$).

The elasticity modulus, thermal expansion, and thermal conductivity for titanium alloy and zirconia are:

The boundary conditions: AB: $u = w = \beta_x = 0$, AD: $v = w = \beta_y = 0$, BC: $u = \beta_x = 0$, CD: $v = \beta_y = 0$.

Titanium alloy: $E_{mt} = 66.2$GPA; $\alpha_{mt} = 10.3 \times 10^{-6}/^\circ$C; $K_{mt} = 18.1$ W/m. K.

Zirconia: $E_{cr} = 244.27$GPa; $\alpha_{cr} = 12.766 \times 10^{-6}/^\circ$C; $K_{cr} = 1.7$ W/m. K.

In the bottom surface, the temperature T_{mt} is assumed to be 25°C. For three variations (uniform, linear and nonlinear) of thermal loading, the CBT difference $\Delta T_{cr} = \Delta T_{cr} \times 10^{-3}$ versus length-thickness aspect ratio L/h is given in Tables 2–4. The power-law indexes are set as $p = 0.5$ and $p = 2$.

The CBT for $p = 2$ is observed to be higher than that for $p = 0.5$ for any thermal loading type.

For $n = L_x/L_y$, the ΔT_{cr} values are shown in Tables 5–7.

The values in each table of the ΔT_{cr} are compared with those of Q4γ_s [55] and Daikh & Megeuni 2017 [56]. It can be seen that the results agree with those of the reference.

Fig. 15 illustrates the ΔT_{cr} variations of the simply supported square plate as a function of the length-thickness ratio L_x/h under the various thermal loading types, three-layer schemes, and power-law indexes $p = 0.5$, 2. The ΔT_{cr} for the plates under UTR is the lowest, while those under NLTR show the highest $\Delta T_{cr.}$ It can be seen that the ΔT_{cr} decreases gradually by increasing the plate aspect ratio L_x/h.

Using the same layer schemes and power-law indexes as in Fig. 15, Fig. 16 shows the ΔT_{cr} versus aspect ratio L_x/L_y under various thermal loading types. The ΔT_{cr} increases gradually by increasing the plate length aspect ratio L_x/L_y. The ΔT_{cr} of the plates under UTR has the lowest value in the different thermal loading conditions.

4. Conclusion

This work focused on formulating the DSQK [5] element for analysing the thermal buckling of three-layer FGM sandwich plates. The strength of the proposed element lies in its simplicity since it is formulated based on FSDT.

The DSQK element of C^0 continuity was proposed based on Reissner-Mindlin first-order shear deformation theory (FSDT). It is a 4-noded element with 5 DOFs per node. To account for the nonlinear distribution of transverse shear stress, a constant shear correction factor $\kappa = 5/6$ was employed. An assumed orthogonality condition for bending energy [7,8] from Bergan's free formulation was adopted to pass the bending patch test. The shear locking, which is normally seen in cases where the FSDT is employed to thin plates, was alleviated by applying the mixed transverse shear strains. For thermal buckling analysis, the strain model of the second-order terms of von Kármán was adopted.

Using the constant curvature patch test and the convergence in the error in the energy norm, the DSQK element's robustness and accuracy were demonstrated. The results from the DSQK element were compared with those from the DSQ [6] and BWQ [7] elements, and it was observed that the DSQK element outperformed the other elements in all test cases considered.

To understand the influence of thermal loading through the thickness on the critical buckling temperature, three different temperature variations, i.e., uniform, linear, and nonlinear temperature increments, were considered. The impact of the material gradient index as determined by the power law model, plate aspect ratio, and thickness ratio was examined, and the results were compared with those from Q4γ_s [55] and Daikh and Megueni [56].

The DSQK element demonstrates reliability and accuracy for both thin and moderately thick plates, with results consistent with those in the existing literature. While it is not suitable for very thick plates where transverse shear effects are very significant, and has not been validated for thickness stretching or FGM distributions beyond the rule of mixture, it remains a simple and effective solution within its validated range. Its straightforward construction also allows for easy implementation using user-element subroutines in commercial finite element software, such as ABAQUS. Future research may extend this approach to alternative material distributions, shell structures, and nonlinear analyses.

CRediT authorship contribution statement

Irwan Katili: Writing – review & editing, Writing – original draft, Validation, Project administration, Methodology, Funding acquisition, Formal analysis, Conceptualization. **Sundararajan Natarajan:** Writing – review & editing, Validation, Supervision. **Magd Abdel Wahab:** Writing – review & editing, Supervision. **Susilo Widyatmoko:** Visualization, Software, Data curation.

Declaration of competing interest

The authors declare that they have no known competing financial interests or personal relationships that could have appeared to influence the work reported in this paper.

Acknowledgements

This research is funded by the Universitas Indonesia (UI), Indonesia through the PUTI Q1 program under grant number NKB-499/UN2.RST/HKP.05.00/2024. The authors gratefully acknowledge this financial support.

Appendix. List of notations

x, y is the Cartesian coordinates systems.
x_i, y_i is the nodal coordinates in Cartesian systems.
ξ, η is the parametric coordinates systems.
ξ_i, η_i is the nodal coordinates i in parametric systems.
n, s is the normal-tangential coordinate systems.
u is the displacement function in x direction
v is the displacement function in y direction
w is the deflection function in z direction
β_x is the rotation in the z-x plane.
β_y is the rotation in the z-y plane.
$w_i, \beta_{x_i}, \beta_{y_i}$ are the DOFs at corner nodes i.
$\Delta\beta_{s_k}$ is the temporary DOFs at each mid-side k of element.
$\langle e\rangle = \langle e_x \quad e_y \quad e_{xy}\rangle$ is the vector of membrane strains.
$\langle \varepsilon\rangle = \langle \varepsilon_x \quad \varepsilon_y \quad \gamma_{xy}\rangle$ is the vector of the von Karman strain buckling model.
$\langle \chi\rangle = \langle \chi_x \quad \chi_y \quad \chi_{xy}\rangle$ is the vector of bending strains.
$\langle \gamma\rangle = \langle \gamma_x \quad \gamma_y\rangle$ are the kinematic transverse shear strains.
$\left\langle \underline{\gamma}\right\rangle = \left\langle \underline{\gamma}_x \quad \underline{\gamma}_y\right\rangle$ are the mixed transverse shear strains.
$\langle M\rangle = \langle M_x \quad M_y \quad M_{xy}\rangle$ is the vector of bending moments.
$\langle T\rangle = \langle T_x \quad T_y\rangle$ is the vector of shear forces.
$[H_m]$ is the constitutive matrix for membrane strains.
$[H_b]$ is the constitutive matrix for bending strains.
$[H_{mb}]$ is the constitutive matrix for a couple of membrane-bending strains.
$[H_s]$ is the constitutive matrix for shear strains.
E is the Young's modulus.
G is the shear modulus.
h is the thickness of the plate.
υ is the Poisson' ratio.
$\kappa = 5/6$ is the shear correction factor.
D_m is the membrane rigidity.
D_b is the bending rigidity.
D_{mb} is the couple membrane-bending rigidity.
D_s is the shear rigidity.
$[J]$ is the Jacobian matrix.
$[j]$ is the inverse of the Jacobian matrix.
$w(s)$ is the deflection function on side i-j along s.
β_s (s) is the rotation function in the z-s plane on side i-j.
C_k and S_k are the direction cosines of side k.
N_i are the linear shape functions at node i ($i = 1, 2, 3, 4$).
P_k are the quadratic shape functions at node k ($k = 5, 6, 7, 8$).
$[B_{b_u}]$ is the l-order bending strains matrix.
$[B_{b_\Delta}]$ is the h-order bending strains matrix.
$[B_m]$ is the membrane strains matrix.
$[B_b]$ is the bending strains matrix.
$[B_{mb}]$ is the couple membrane-bending strains matrix.
DOFs: degree of freedoms.
$\langle u_n\rangle$ is the DOFs element.
$\langle \Delta\beta_n\rangle$ is the vector of temporary DOFs.
$\prod_{int}^{b}$ the bending energy.
$\prod_{int}^{b}(l\text{ - order})$ is the l-order (lower-order) bending energy.
$\prod_{int}^{b}(c\text{ - order})$ is the c-order (couple-order) bending energy.
$\prod_{int}^{b}(h\text{ - order})$ is the h-order (higher-order) bending energy.
$\prod_{int}^{mb}$ is the couple membrane-bending energy.
$\prod_{int}^{s}$ is the transverse shear energy.
Π_{int}^{σ} The membrane strain energy of the von Kármán model.
$[k_{b_u}]$ is the l-order bending stiffness.
$[k_{b_{u\Delta}}]$ is the c-order bending stiffness.
$[k_{b_\Delta}]$ is the h-order bending stiffness.
$[k_b]$ is the bending stiffness.
$[k_s]$ is the transverse shear stiffness.
$[k_m]$ is the membrane stiffness.

$[k_G]$ The geometric stiffness of the von Kármán model.
γ_s is the kinematic transverse shear strain on side k.
$\underline{\gamma}_{s_k}$ is the constant transverse shear strain on side k.
$E^n(z)$ is the distribution of Young's modulus in n-layer.
E_{cr} is the Young's modulus of ceramic.
E_{mt} is the Young's modulus of metal.
$\alpha^n(z)$ is the distribution of thermal expansion coefficient in n-layer.
α_{mt} is the coefficient of metal thermal expansion
α_{cr} is the coefficient of ceramic thermal expansion
FGM functionally graded material.
$K^n(z)$ is the distribution of thermal conductivity coefficient in n-layer.
K_{mt} is the coefficient of metal thermal conductivity.
K_{cr} is the coefficient of ceramic thermal conductivity.
$V^n_{cr}(z)$ is the volume fraction of ceramic at n-layer.
$V^n_{mt}(z)$ is the volume fraction of metal at n-layer.
N_{cr} is the buckling load parameter.
ΔT_{up} is the upper surface temperature changes of the plates.
ΔT_{lw} is the lower surface temperature changes of the plates.
ΔT_{cr} is the critical buckling temperature change.
UTR: Uniform temperature rise.
LTR: Linear temperature rise.
NLTR: Non-linear temperature rise.
E_R is the error in norm energy norm.
$\|\Pi^{\mathrm{Ex}}_{\mathrm{int}}\|^2$ is the analytical solution of the strain energy.
$\|\Pi^{\mathrm{FE}}_{\mathrm{int}}\|^2$ is the result of the finite element model.

Data availability

All data have been included in the manuscript

References

[1] Koizumi M. The concept of FGM. Ceram Trans Funct Grad Mater 1993;34:3–10.
[2] Kirchhoff G. Uber das Gleichgewicht und die Bewegung einer, elastischen Scheib. J Reine Angew Math 1950;40:51–8.
[3] Reissner E. The effect of transverse shear deformation on the bending of elastic plates. J Appl Mech 1945;12:A69–77.
[4] Mindlin RD. Influence of rotatory inertia and shear of flexural motions of isotropic elastic plates. J Appl Mech 1951;18:31–8.
[5] Katili I. An improved incompatible DSQ element using free formulation approach. Struct Eng Mech 2021;78:665–79.
[6] Lardeur P., "Développement et évaluation de deux nouveaux éléments finis de plaques et coques composites avec influence du cisaillement transversal", Ph.D. Dissertation 1990, UTC, Compiègne-France.
[7] Bergan PG, Wang X. Quadrilateral plate bending elements with shear deformations". Comput Struct 1984;19:25–34.
[8] Felippa CA, Bergan PG. A triangular bending element based on an energy orthogonal free formulation. Comput Methods Appl Mech Eng 1987;61:129–60.
[9] Bathe KJ, Dvorkin EN. A four-node plate bending element based on Mindlin-Reissner plate theory and a mixed interpolation. Int J Numer Meth Eng 1985;21: 367–83.
[10] Ayad R, Dhatt G, Batoz JL. A new hybrid-mixed variational approach for Reissner-Mindlin plates: the MiSP Model. Int J Numer Meth Eng 1998;42:1149–79.
[11] Lee PS, Bathe KJ. Development of MITC isotropic triangular shell finite elements. Comput Struct 2004;82:945–62.
[12] Ko Y, Lee PS, Bathe KJ. The MITC4+ shell element and its performance. Comput Struct 2016;169:57–68.
[13] Ko Y, Lee PS, Bathe KJ. A new MITC4+ shell element. Comput Struct 2017;182: 404–18.
[14] Katili I, Maknun IJ, Katili AM, Bordas SP, Natarajan S. A unfied polygonal lockingfree thin/thick smoothed plate element. Compos Struct 2019;219:147–57.
[15] Batoz JL, Antaluca E, Katili I. On the formulation and evaluation of old and new efficient low order triangular plate bending elements with shear effects. Comput Mech 2021;68:69–96.
[16] Katili AM, Bletzinger KU, Katili I. An optimum triangular plate element based on DSPM with incomplete quadratic functions and an assumed orthogonality condition. Comput Struct 2024;296:107301.
[17] Batoz JL, Katili I, Widyatmoko S, Antaluca E. An efficient shear and bending-locking-free quadrilateral plate element using a modified Hellinger-Reissner functional and the Bergan free formulation. Int J Numer Meth Eng 2024;125:7451.
[18] Akhila G, Sundararajan NS, Lian H, Katili I. Locking-free polygonal plate element based on the discrete shear projection method. Comput Struct 2025;309:107661.
[19] Katili AM, Bletzinger KU, Katili I. An enrichment of Q4γs plate finite element using incomplete quadratic functions, an assumed energy orthogonality of Bergan's free formulation, and mixed transverse shear strains. Comput Struct 2025;307:107619.
[20] Katili I, Batoz JL, Maknun IJ, Katili AM. On static and free vibration analysis of FGM plates using an efficient quadrilateral finite element based on DSPM. Compos Struct 2021;261:113514.
[21] Katili AM, Katili I. Improving the Bergan Wang Quadrilateral plate element by using the UI approach for analysis of isotropic and FGM sandwich plates. Thin-Walled Struct 2023;18:110328.
[22] Katili I, Batoz JL, Bouabdallah S, Maknun IJ, Katili AM. Discrete shear projection method for mechanical buckling analysis of FGM sandwich plates. Compos Struct 2023;312:116825.
[23] Thai HT, Nguyen TK, Vo TP, Lee J. Analysis of functionally graded sandwich plates using a new first-order shear deformation theory. Eur J Mech-A/Solids 2014;45: 211–25.
[24] Bennoun M, Houari MSA, Tounsi A. A novel five-variable refined plate theory for vibration analysis of functionally graded sandwich plates. Mech Adv Mater Struct 2016;23:423–31.
[25] Thai CH, Zenkour AM, Wahab MA, Nguyen-Xuan H. A simple four-unknown shear and normal deformations theory for functionally graded isotropic and sandwich plates based on isogeometric analysis. Compos Struc 2016;139:77–95.
[26] Cheng ZQ, Batra RC. Deflection relationships between the homogeneous Kirchhoff plate theory and different functionally graded plate theories. Arch Mech 2000;52: 143–58.
[27] Cheng ZQ, Batra RC. Three-dimensional thermoelastic deformations of a functionally graded elliptic plate. Compos B Eng 2000;31:97–106.
[28] Cheng ZQ, Batra RC. Exact correspondence between eigenvalues of membranes and functionally graded simply supported polygonal plates. J Sound Vib 2000;229: 879–95.
[29] Zenkour AM. A comprehensive analysis of functionally graded sandwich plates: Part 1-deflection and stresses. Int J Solids Struct 2005;42:5224–42.
[30] Zenkour AM. A comprehensive analysis of functionally graded sandwich plates: Part 2 - buckling and free vibration. Int J Solids Struct 2005;42:5243–58.
[31] Mantari JL, Granados EV. A refined FSDT for the static analysis of functionally graded sandwich plates. Thin-Walled Struct 2015;90:150–8.
[32] Reddy JN. A refined nonlinear theory of plates with transverse shear deformation. Int J Solids Struct 1984;20:881–96.
[33] Reddy JN, Pan ND. Stability and vibration of isotropic, orthotropic and laminated plates according to a higher–order shear deformation theory. J Sound Vib 1985;98: 157–70.
[34] Reddy JN. analysis of functionally graded plates. Int J Numer Meth Eng 2000;47: 663–84.
[35] Carrera E. A priori vs. a posteriori evaluation of transverse stresses in multilayered orthotropic plates. Compos Struct 2000;48:245–60.
[36] Neves AMA, Ferreira AM, Carrera E, Roque CMC, Cinefra M, Jorge RMN, et al. A quasi-3D sinusoidal shear deformation theory for the static and free vibration analysis of functionally graded plates. Compos B Eng 2012;43:711–25.
[37] Neves AMA, Ferreira AJM, Carrera E, Cinefra M, Jorge RMN, Soares CMM. Buckling analysis of sandwich plates with functionally graded facesheets using a

new quasi-3D hyperbolic sine shear deformation theory and collocation with radial basis functions. J Appl Math Mech 2012;92:749–66.
[38] Neves AMA, Ferreira AJM, Carrera E, Cinefra M, Jorge RMN, Soares CMM. Static analysis of functionally graded sandwich plates according to a hyperbolic theory considering zig-zag and warping effects. Adv Eng Softw 2012;52:30–43.
[39] Neves AMA, Ferreira AJM, Carrera E, Cinefra M, Roque CMC, Jorge RMN, et al. A quasi-3D hyperbolic shear deformation theory for the static and free vibration analysis of functionally graded plates. Compos Struct 2012;94:1814–25.
[40] Neves AMA, Ferreira AJM, Carrera E, Cinefra M, Roque CMC, Jorge RMN, et al. free vibration and buckling analysis of isotropic and sandwich functionally graded plates using a quasi-3D higher-order shear deformation theory and a meshless technique. Compos B Eng 2013;44:657–74.
[41] Tounsi A, Houari MSA, Benyoucef S, Bedia EAA. A refined trigonometric shear deformation theory for thermoelastic bending of functionally graded sandwich plates. Aero Sci Technol 2013;24:209–20.
[42] Nguyen VH, Nguyen TK, Thai HT, Vo TP. A new inverse trigonometric shear deformation theory for isotropic and functionally graded sandwich plates. Compos B Eng 2014;66:233–46.
[43] Mahi A, Bedia EAA, Tounsi A. A new hyperbolic shear deformation theory for bending and free vibration analysis of isotropic, functionally graded, sandwich and laminated composite plates. J Appl Math Mech 2015;39:2489–508.
[44] Pandey S, Pradyumna S. A new C0 higher-order layerwise finite element formulation for the analysis of laminated and sandwich plates. Compos Struct 2015;131:1–16.
[45] Pandey S. Pradyumna, analysis of functionally graded sandwich plates using a higher-order layerwise theory. Compos B Eng 2018;153:325–36.
[46] Carrera E, Zozulya VV. Carrera Unified Formulation (CUF) for the composite plates and shells of revolution. Compos Struct 2024;334:117936.
[47] Demasi L, Ashenafi Y, Cavallaro R, Santarpia E. Generalized Unified Formulation shell element for functionally graded Variable-Stiffness Composite Laminates and aeroelastic applications. Compos Struct 2015;131:501–15.
[48] D'Ottavio M. A Sublaminate generalized unified formulation for the analysis of composite structures. Compos Struct 2016;142:187–99.
[49] Javaheri R, Eslami MR. Thermal Buckling of Functionally Graded Plates. AIAA J 2002;40:162–9.
[50] Javaheri R, Eslami MR. Thermal Buckling of Functionally Graded Plates based on Higher order Theory. J Therm Stresses 2002;25:603–25.
[51] Shariat BAS, Eslami MR. Buckling of thick functionally graded plates under mechanical and thermal loads. Compos Struct 2007;78:433–9.
[52] Zenkour AM, Alghamdi NA. Thermoelastic bending analysis of functionally graded sandwich plates. J Mater Sci 2008;43(8):2574–89.
[53] Li D, Deng Z, Chen G, Xiao H, Zhu L. Thermomechanical bending analysis of sandwich plates with both functionally graded face sheets and functionally graded core. Comput Struct 2017;169:29–41.
[54] Trinh MC, Kim SE. Nonlinear thermomechanical behaviors of thin functionally graded sandwich shells with double curvature. Compos Struct 2018;195:335–48.
[55] Katili I, Batoz JL, Widyatmoko S, Naceur H. The Q4γs plate finite element for three-layer FGM sandwich plates in deflection, stresses, vibration, and thermal buckling analysis. Compos Struct 2024;338:118098.
[56] Daikh AA, Megueni A. Thermal buckling analysis of functionally graded sandwich plates. J Therm Stresses 2017;41:139–59.